Int J Adv Manuf Technol (2015) 77:1387–1399
DOI 10.1007/s00170-014-6559-z

ORIGINAL ARTICLE

Investigation and modeling of cutting forces and surface roughness when hard turning of AISI 52100 steel with mixed ceramic tool: cutting conditions optimization

I. Meddour · M. A. Yallese · R. Khattabi · M. Elbah · L. Boulanouar

Received: 25 May 2014 / Accepted: 27 October 2014 / Published online: 9 November 2014
© Springer-Verlag London 2014

Abstract The increasing industrial demand for hard materials and their wide range of applications requires significant investigations to improve their machinability. Therefore, the current study addresses cutting forces and surface roughness during hard turning of AISI 52100 steel (59 hardness Rockwell C (HRC)) using ceramic tool. Turning experiments were held out by varying cutting speed, depth of cut, feed rate, and tool nose radius. For so doing, a central composite design (CCD) was adopted including 30 tests. Cutting forces and surface roughness were modeled using response surface methodology (RSM). The effects of each input parameter on output responses were investigated using analysis of variance (ANOVA) and response surface graphics. The findings of this study demonstrated that the force components were significantly influenced by depth of cut, followed by feed rate with a lower degree. Likewise, the negative result of the small undeformed chip thickness on surface roughness was reduced by the employment of large nose radius. Conclusively, a correlation between cutting force behavior and surface roughness was established and confirmed by the three-dimensional topographic maps of the machined surfaces. The RSM was utilized to define the optimal machining parameters.

Keywords Hard turning · ANOVA · RMS · Surface roughness · Cutting force · Optimization

I. Meddour (✉) · M. A. Yallese · R. Khattabi · M. Elbah
Mechanics and Structures Research Laboratory (LMS),
May 8th 1945 University, P.O. Box 401, 24000 Guelma, Algeria
e-mail: meddour26@yahoo.fr

L. Boulanouar
Research Laboratory of Advanced Technology in Production Engineering (RLATPE), Badji Mokhtar University,
P.O. Box 12, 23000 Annaba, Algeria

1 Introduction

To replace grinding operations and gain some advantages, hard turning is widely used in industry. It consists of machining parts in which hardness exceeds 45 hardness Rockwell C (HRC). It reduces the time of machine setup and keeps off the lubrication. This alternative represents a significant material removal rates and keeps an improved surface finish with a better fatigue performance [1]. Hard turning requires the use of inserts that offer a high wear resistance and a chemical stability at high temperature. Those features are found in cubic boron nitride (CBN), polycrystalline cubic boron nitride (PCBN), and ceramic tool inserts. Basically, ceramic tool represents an economical alternative due to its lower price compared to CBN. The study of the different phenomena (surface integrity, tool wear, cutting forces, and chip formation) which are produced during the process is needed for equipment design and the improvement of productivity and quality of the machined products. In addition to that, the prediction of surface roughness and cutting forces is becoming important in the area of hard turning as well. Benga and Abrao [2] used the response surface methodology (RSM) to investigate the surface roughness of hard turned bearing steel (100Cr6) with mixed ceramic, whisker-reinforced ceramic, and PCBN inserts. Cutting speed and feed rate were considered as variable parameters. The results showed that the surface roughness was affected by feed rate for the three cutting tool types. The same effect of feed rate was detected by Kacal and Yildirim [3] during hard turning of AISI D6 cold work tool steel with ceramic and CBN inserts. They applied the gray relational analysis (GRA) to optimize the cutting conditions for surface roughness, cutting power, tool wear, and specific cutting force. When turning hardened AISI 4140 steel with mixed ceramic inserts, the analysis of variance (ANOVA) results employed by Aslan et al. [4] revealed that the surface roughness was mainly influenced by cutting

speed-feed rate and feed rate-depth of cut interactions. In the case of AISI H11 steel hard turned with coated mixed ceramic inserts, the RSM was employed for the optimization approach by Dureja et al. [5]. Also, they concluded by applying RSM plot that the best surface roughness was attainable at a small feed rate and high cutting speed. This combination of feed rate and cutting speed was also suggested by Ozel et al. [6] in finish turning of AISI D2 steels using wiper ceramic inserts. They developed a multiple linear regression models and neural network models to predict surface roughness. Conversely, the surface roughness of AISI 52100 steel that was machined with CBN tool decreased while the feed increased. It was assigned to the ploughing instead of cutting [7]. A new optimization approach called the multivariate robust parameter design (MRPD) was applied by Paiva et al. [8] with the target of minimal surface roughness during hard turning of AISI 52100 steel with coated mixed ceramic inserts. In a recent study, Satyanarayana et al. [9] used the ANOVA to evaluate the significance of cutting parameters and rake angle on cutting force and surface roughness obtained in hard turning of titanium alloy.

Other experimental studies were focused on tool geometry effects as the work of Thiele and Melkote [10]. They found that CBN cutting edge geometry and workpiece hardness are statistically significant on surface roughness and cutting forces in finish turning of AISI 52100 steel. The influence of tool nose radius, approach angle, and rake angle on surface finish was investigated by Neseli et al. [11]. They indicated that the tool nose radius was the prevailing component. Elbah et al. [12] compared between the values of surface roughness obtained by wiper ceramic inserts with those obtained by conventional ceramic inserts during hard turning of AISI 4140 steel. They disclosed that the improved surface quality is achieved with wiper geometry. The same report was done by Guddat et al. [13] in hard turning of AISI 52100 steel with PCBN wiper inserts. However, higher values of compressive residual stresses were registered.

As the conditions of machining hard material change from those in conventional turning, they involve a change in cutting force behavior. Hence, a large number of researchers reported that the thrust force was the largest one among the cutting force components. Some of them linked this dominance to the very small depth of cut and large negative rake angle [14–17]. Nakayama et al. [18] observed that a great thrust force caused elastic deformation in cutting zone that led to a dimensional error on machined workpiece. Deep explanation regarding this matter was made by Astakhov [19]. He bound up the dominance of thrust force to the spring back of the machined surface. Bouacha et al. [20] demonstrated that the evolution of thrust force as function of workpiece hardness was considerable. Chou and Song [21] reported that a large nose radius with the rake angle (−25°) increased the force components and improved the surface finish in hard turning of AISI 52100 steel with ceramic tool. Kurt and Seker [22] found that the chamfer angle of PCBN insert influences the thrust force to a greater extent than the tangential one.

It is well recognized that the cutting forces decrease when hard turning at low cutting speeds. Furthermore, low cutting speeds could encourage the creation of the built-up edge (BUE) which deteriorates the surface roughness. The BUE increases the dynamic forces, the risk of excessive chipping, and the fracture of the brittle ceramic tool [4]. On the other hand, at high cutting speeds, the cutting force components decrease because of temperature elevation which brings down the shear force of the study stuff. Bouacha et al. [20] observed in their experimental study that the thrust force is much more influenced by the cutting speed. In hard turning of AISI 52100 steel with CBN tool, Bagawade et al. [23] revealed that force components were principally affected by cutting speed and depth of cut, whereas the feed rate was insignificant.

Compared to the above-mentioned investigations concerning hard turning of AISI 52100 steel using mixed ceramic tools, this experimental study is realized to investigate the effect of a large number of parameters and their interactions on the cutting forces and surface roughness. The parameters investigated include the following: cutting speed, depth of cut, feed rate, and insert geometry, i.e., tool nose radius, with value variation allowing precision hard turning. Additionally, the modeling of cutting forces and surface roughness is performed using RSM. The final goal of this work is the optimization of the cutting conditions.

2 Experimental procedure

2.1 Equipment

The experimental tests are performed under dry conditions using AISI 52100 steel as workpiece material. The hardness was raised by quenching and tempering treatment followed by checking measurement with a digital Micron Hardness Tester DM2-D390. The average of measured values was 59 HRC. The chemical composition of the workpiece is given in Table 1.

Table 1 Chemical composition of AISI 52100 steel

Element	C	Cr	Al	Mn	Si	Cu	Mo	Sn	P	Ni	V
Amount (%)	1.05	1.41	0.03	0.38	0.21	0.28	0.02	0.02	0.02	0.21	0.01

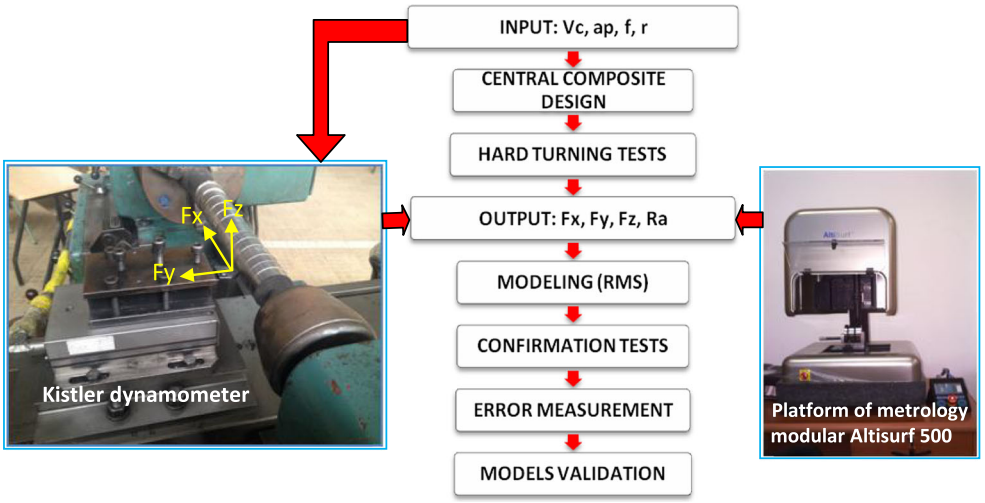

Fig. 1 Modeling process

A universal lathe is used for machining operations, model SN40C, spindle power 6.6 kW. The measurement of cutting forces is done by three-axial dynamometer (Kistler 9257B) mounted in the tool holder (Fig. 1). It is connected to a multichannel charge amplifier (type 5011 B) and data acquisition system. The ceramic insert tool which offers eight cutting edges is a mix of 70 % Al_2O_3 and 30 % TiC. This type of inserts is commonly called CC650, and its physical properties are presented in Table 2. Its ISO designation is SNGN 1204(r) T01020 where (r) is the tool nose radius ranged from 0.8 to 1.6 mm in this work, indicating a 20° chamfer angle over 0.1-mm width. The insert is clamped to a tool holder codified as PSBNR 2525 M12 with a common active part tool geometry described by the following: cutting edge angle χr=75°, clearance angle α=6°, rake angle γ=−6, and cutting edge inclination angle λ=−6. A new cutting edge is used for each test in order to reduce the wear influence on measured responses.

Regarding the measurement of the surface roughness, a Mitutoyo Surftest 201 (cutoff=0.8) is applied after each test in three different positions by going around the workpiece each 120°. Afterward, the average of the three measurements is calculated. Additionally, the three-dimensional topographic maps of the machined surfaces are produced using the optical platform of metrology modular Altisurf 500 (Fig. 1).

2.2 Experimental design

The experimental approach is adopted with the purpose of studying the effects of the different factors and their interaction by varying them in a controlled manner. For that, the experimental tests are carried out according to a central composite design (CCD). The choice of this figure is made with great attentiveness to time consumption and cost. Thirty experimental runs composed of 16 factorial points, six center points, and eight axial points are carried out. In order to get three levels of each factor, tests are realized on cube surface which means α=1. The independent variables are as follows: cutting speed (Vc), feed rate (f), cutting depth (ap), and tool noise radius (r). The level's factors are presented in Table 3. The responses are as follows: feed force (Fx), thrust force (Fy), tangential force (Fz), and the arithmetic mean of roughness (Ra).

The principal of the RMS is to model the experimental data. The CCD allows the evaluation of the linear effects and also to the eventual quadratic interaction effects between the different variables. We apply the quadratic model with interactions as follows:

$$Y = a_0 + \sum_{i=1}^{k} b_i X_i + \sum_{i,j}^{k} b_{ij} X_i X_j + \sum_{i=1}^{k} b_{ii} X_i^2 \quad (1)$$

where i, j, k=1, 2… n a_0, b_i, b_{ij}, and b_{ii} are the regression coefficients of the model and X_i and X_j, are the explicative variables. The ANOVA was employed in order to determine the significance of the independent variables on the output responses. The results of the experimental tests are presented in Table 4.

Table 2 Physical properties of ceramic CC650

Cutting material	Vickers hardness (daN/mm^2)	Tenacity (MPa m$^{1/2}$)	Young's modulus (GPa)	Density (g/cm^2)	Grain size (μm)	Thermal conductivity (W/m K)
Ceramic CC650	1900	4.0	410	4.15	2.0	28

Table 3 Factors variation

level	Cutting speed (m/min)	Feed rate (mm/rev)	Depth of cut (mm)	Tool nose radius (mm)
−1	100	0.08	0.05	0.8
0	150	0.11	0.15	1.2
+1	200	0.14	0.25	1.6

3 Results and discussion

3.1 Statistical analysis and modeling

The regression equations are generated by Design Expert software (Version 8.0.7). Those equations describe the statistical relationship between the factors and the responses and could predict new runs. The ANOVA is performed to establish the statistical significance of the regression models, model terms, and lack of fit. It is done by comparing "Prob > *F*" to 0.05 or in other words at 95 % of confidence. Tables 5, 6, 7, 8, and 9 show that the cutting force components and surface roughness models are significant with Prob > *F* values less than 0.0001. The proportion of contribution of each model term was calculated.

3.1.1 Feed force (Fx)

According to ANOVA results of feed force presented in Table 5, the term *ap* represents the higher statistical significance on feed force with the contribution of 79.85 %. The term *f* is also significant with smaller contribution of 6.02 %.

Table 4 Experimental run and results

	Input variables				Output responses			
Run	*Vc* (m/min)	*ap* (mm)	*f* (mm/rev)	*r* (mm)	*Fx* (N)	*Fy* (N)	*Fz* (N)	*Ra* (μm)
01	100	0.25	0.08	1.6	33.18	98.31	102.70	0.33
02	200	0.05	0.08	0.8	2.18	55.83	18.16	0.65
03	150	0.05	0.11	1.2	10.21	31.76	23.25	0.59
04	150	0.15	0.08	1.2	29.37	102.47	80.33	0.37
05	150	0.15	0.11	1.6	18.74	93.90	89.80	0.41
06	150	0.25	0.11	1.2	32.38	73.82	116.14	0.63
07	200	0.25	0.08	1.6	27.38	92.55	84.51	0.30
08	100	0.05	0.14	0.8	11.93	52.39	42.39	1.09
09	200	0.25	0.14	1.6	34.64	122.48	132.5	0.44
10	150	0.15	0.11	1.2	22.60	74.34	69.96	0.59
11	200	0.15	0.11	1.2	21.14	95.39	84.36	0.54
12	200	0.05	0.14	1.6	24.43	73.57	53.35	0.37
13	200	0.05	0.14	0.8	12.95	44.26	34.29	0.98
14	200	0.05	0.08	1.6	5.84	30.91	25.26	0.34
15	150	0.15	0.14	1.2	33.32	103.94	100.75	0.61
16	100	0.05	0.14	1.6	4.13	72.41	49.69	0.45
17	200	0.25	0.08	0.8	32.75	67.12	93.84	0.37
18	150	0.15	0.11	1.2	32.70	65.43	81.32	0.54
19	100	0.05	0.08	1.6	3.50	50.45	40.29	0.31
20	100	0.25	0.14	1.6	34.30	128.33	138.06	0.62
21	100	0.25	0.14	0.8	49.04	111.04	142.54	0.79
22	200	0.25	0.14	0.8	38.99	102.36	132.18	0.83
23	150	0.15	0.11	0.8	28.66	76.59	73.13	0.61
24	150	0.15	0.11	1.2	35.66	90.14	71.93	0.53
25	150	0.15	0.11	1.2	28.90	71.03	73.85	0.53
26	100	0.25	0.08	0.8	39.22	80.39	90.36	0.35
27	100	0.15	0.11	1.2	29.16	87.98	85.49	0.45
28	100	0.05	0.08	0.8	4.01	31.17	23.73	0.64
29	150	0.15	0.11	1.2	29.69	89.19	64.78	0.48
30	150	0.15	0.11	1.2	23.72	78.12	93.67	0.56

Table 5 ANOVA for response surface quadratic model for *Fx*

Source	Sum of squares	*df*	Mean square	*F* value	Prob	Observation	Cont.%
Model	4219.01	14	301.36	15.77	<0.0001	Significant	
A—*Vc*	3.31	1	3.31	0.17	0.6831	Not significant	0.08
B—*ap*	3284.55	1	3284.55	171.88	<0.0001	Significant	79.85
C—*f*	247.53	1	247.53	12.95	0.0026	Significant	6.02
D—*r*	64.37	1	64.37	3.37	0.0864	Not significant	1.56
AB	122.43	1	122.43	6.41	0.0230	Significant	2.98
AC	32.83	1	32.83	1.72	0.2096	Not significant	0.80
AD	76.39	1	76.39	4.00	0.0640	Not significant	1.86
BC	12.11	1	12.11	0.63	0.4384	Not significant	0.29
BD	85.01	1	85.01	4.45	0.0522	Not significant	2.07
CD	2.81	1	2.81	0.15	0.7070	Not significant	0.07
A^2	6.78	1	6.78	0.35	0.5604	Not significant	0.16
B^2	77.58	1	77.58	4.06	0.0622	Not significant	1.89
C^2	54.30	1	54.30	2.84	0.1125	Not significant	1.32
D^2	24.37	1	24.37	1.28	0.2765	Not significant	0.59
Residual	286.65	15	19.11				0.46
Lack of fit	159.37	10	15.94	0.63	0.7531	Not significant	
Pure error	127.28	5	25.46				
Cor total	4505.66	29					
Std. dev.	4.37	R^2	0.9364				
Mean	24.48	Adj R^2	0.8770				
C.V. %	17.86	Pred R^2	0.7487				
Press	1132.36	Adeq Precision	14.640				

df degrees of freedom, *Cont.%* percentage contribution ratio (%)

On the other hand, the cutting speed (*Vc*) and the tool nose radius (*r*) do not present any statistical significance. The interaction $Vc \times ap$ is significant with slight contribution of 2.98 %. The lack-of-fit *p* value of 0.7531 was greater than 0.05. Therefore, the regression model does not fail to adequately explain the functional relationship between the experimental factors and the response. Lack of fit may occur if important terms from the model such as interactions or quadratic terms are not included. The correlation coefficient R^2 of about 0.9364 is considered good. It represents the proportion of variation in the response which is explained by the model. The "Pred R^2" of 0.7487 is in reasonable agreement with the "Adj R^2" of 0.8770.

The final equation in terms of real factors of feed force is given as follows:

$$Fx = 11.211 + 0.032Vc + 483.284ap - 1053.305f + 37.374r - 0.553Vc \times ap + 0.955Vc \times f + 0.109Vc \times r - 290ap \times f - 57.625ap \times r - 34.896f \times r - 0.001Vc^2 - 547.211ap^2 + 5086.55f^2 - 19.169r^2 \quad (2)$$

3.1.2 Thrust force (Fy)

The ANOVA results of thrust force presented in Table 6 show that the most significant model term is *ap* with 57.62 % of contribution, followed by *f* with lower contribution of 12.45 %. The term *r* appears especially significant on thrust force. Its contribution is 6.16 %. Similarly, Meng [14] observed that the effect of the nose radius was so notable on thrust force. The quadratic term ap^2 is significant with 14.35 % of contribution. The coefficient R^2 of about 0.91 is considered good, but the Pred R^2 of 0.539 which represents the efficiency of the model to expect new runs is not as close to the Adj R^2 of 0.8145. This leads to consider a model reduction by backward elimination. The results of backward elimination process are presented in Table 7. It shows that in addition to the terms cited above, the term f^2 becomes significant with 9.18 % of contribution. The Pred R^2 is improved to 0.7994, and it is in reasonable agreement with the Adj R^2 of

Table 6 ANOVA for response surface quadratic model for *Fy*

Source	Sum of squares	*df*	Mean square	*F* value	Prob	Observation	Cont.%
Model	17,316.82	14	1236.92	10.86	<0.0001	Significant	
A—*Vc*	43.56	1	43.56	0.38	0.5457	Not significant	0.24
B—*ap*	10,447.35	1	10,447.35	91.70	<0.0001	Significant	57.62
C—*f*	2257.47	1	2257.47	19.81	0.0005	Significant	12.45
D—*r*	1116.44	1	1116.44	9.80	0.0069	Significant	6.16
AB	62.85	1	62.85	0.55	0.4691	Not significant	0.35
AC	3.60	1	3.60	0.032	0.8613	Not significant	0.02
AD	37.73	1	37.73	0.33	0.5735	Not significant	0.21
BC	166.22	1	166.22	1.46	0.2458	Not significant	0.92
BD	85.89	1	85.89	0.75	0.3989	Not significant	0.47
CD	150.25	1	150.25	1.32	0.2688	Not significant	0.83
A^2	134.34	1	134.34	1.18	0.2947	Not significant	0.74
B^2	2602.64	1	2602.64	22.84	0.0002	Significant	14.35
C^2	908.02	1	908.02	7.97	0.0128	Not significant	5.01
D^2	1.50	1	1.50	0.013	0.9102	Not significant	0.01
Residual	17,316.82	15	113.93				0.63
Lack of fit	43.56	10	121.64	1.23	0.4317	Not significant	
Pure error	10,447.35	5	98.52				
Cor total	2257.47	29					
Std. dev.	10.67	R^2	0.9102				
Mean	78.26	Adj R^2	0.8263				
C.V. %	13.64	Pred R^2	0.5390				
Press	8770.27	Adeq Precision	14.321				

0.8476. The final equation in terms of real factors resulted from the backward elimination process is given as follows:

$$Fy = 213.982 + 1091.586ap - 5018.990f + 19.689r - 2835.565ap^2 + 24510.394f^2 \quad (3)$$

3.1.3 Tangential force (Fz)

The ANOVA results of tangential force presented in Table 8 indicate that *ap* is significant with the largest contribution of 83.12 %. The next term influencing the

Table 7 ANOVA for response surface reduced quadratic model for *Fy*

Source	Sum of squares	*df*	Mean square	*F* value	Prob	Observation	Cont.%
Model	16,608.72	5	3321.74	33.2593	<0.0001	Significant	
B—*ap*	10,447.35	1	10,447.35	103.5104	<0.0001	Significant	56.88
C—*f*	2257.47	1	2257.47	23.7273	<0.0001	Significant	12.29
D—*r*	1116.44	1	1116.44	12.279	0.0028	Significant	6.08
B^2	2769.48	1	2769.48	26.7205	<0.0001	Significant	15.08
C^2	1676.12	1	1676.12	15.2239	0.0004	Significant	9.13
Residual	2417.07	24	100.71				0.55
Lack of fit	1924.49	19	101.29	1.1011	0.5407	Not significant	
Pure error	492.58	5	98.52				
Cor total	19,025.79	29					
Std. dev.	10.04	R^2	0.8730				
Mean	78.26	Adj R^2	0.8465				
C.V. %	12.82	Pred R^2	0.7997				
Press	3811.60	Adeq Precision	19.901				

Table 8 ANOVA for response surface quadratic model for *FZ*

Source	Sum of squares	*df*	Mean square	*F* value	Prob	Observation	Cont.%
Model	34,737.14	14	2481.22	34.64	<0.0001	Significant	
A—*Vc*	179.24	1	179.24	2.50	0.1345	Not significant	0.51
B—*ap*	28,993.93	1	28,993.93	404.78	<0.0001	Significant	83.12
C—*f*	3947.75	1	3947.75	55.11	<0.0001	Significant	11.32
D—*r*	238.64	1	238.64	3.33	0.0879	Not significant	0.68
AB	1.95	1	1.95	0.027	0.8711	Not significant	0.01
AC	13.97	1	13.97	0.20	0.6651	Not significant	0.04
AD	13.27	1	13.27	0.19	0.6730	Not significant	0.04
BC	645.03	1	645.03	9.01	0.0090	Significant	1.85
BD	163.65	1	163.65	2.28	0.1514	Not significant	0.47
CD	1.25	1	1.25	0.017	0.8967	Not significant	0.00
A^2	14.60	1	14.60	0.20	0.6581	Not significant	0.04
B^2	428.23	1	428.23	5.98	0.0273	Significant	1.23
C^2	165.36	1	165.36	2.31	0.1495	Not significant	0.47
D^2	3.06	1	3.06	0.043	0.8391	Not significant	0.01
Residual	1074.43	15	71.63				0.21
Lack of fit	550.39	10	55.04	0.53	0.8194	Not significant	
Pure error	524.05	5	104.81				
Cor total	35,811.57	29					
Std. dev.	8.46	R^2	0.9700				
Mean	77.09	Adj R^2	0.9420				
C.V. %	10.98	Pred R^2	0.8996				
Press	3594.36	Adeq Precision	20.633				

Table 9 ANOVA for response surface 2fi model for *Ra*

Source	Sum of squares	*df*	Mean square	*F* value	Prob	Observation	Cont.%
Model	0.99	10	0.099	29.09	<0.0001	Significant	
A—*Vc*	2.450E−3	1	2.450E−3	0.72	0.4075	Not significant	0.25
B—*ap*	0.032	1	0.032	9.40	0.0064	Significant	3.22
C—*f*	0.35	1	0.35	103.30	<0.0001	Significant	35.39
D—*r*	0.42	1	0.42	122.13	<0.0001	Significant	41.83
AB	0.000	1	0.000	0.000	1.0000	Not significant	0.00
AC	8.100E−3	1	8.100E−3	2.37	0.1400	Not significant	0.81
AD	3.025E−3	1	3.025E−3	0.89	0.3584	Not significant	0.30
BC	9.025E−3	1	9.025E−3	2.64	0.1205	Not significant	0.91
BD	0.096	1	0.096	28.14	<0.0001	Significant	9.64
CD	0.073	1	0.073	21.35	0.0002	Significant	7.31
Residual	0.065	19	3.415E−3				0.34
Lack of fit	0.058	14	4.158E−3	3.11	0.1082	Not significant	
Pure error	6.683E−3	5	1.337E−3				
Cor total	1.06	29					
Std. dev.	0.058	R^2	0.9387				
Mean	0.54	Adj R^2	0.9064				
C.V. %	10.76	Pred R^2	0.8335				
Press	0.18	Adeq Precision	20.213				

tangential force is f with 11.32 % of contribution. The terms $ap \times f$ and ap^2 are also significant with slight contribution. The determination coefficient model's R^2 is 0.9700. The Pred R^2 of 0.8996 is in reasonable agreement with the Adj R^2 of 0.9420.

The final equation in terms of real factors is given as follows:

$$Fz = 71.311 - 0.351Vc + 660.643ap - 1842.153f + 46.778r - 0.07Vc \times ap + 0.623Vc \times f - 0.046Vc \times r + 2116.458ap \times f - 79.953ap \times r - 23.281f \times r + 0.001Vc^2 - 1285.614ap^2 + 8876.511f^2 - 6.788r^2 \quad (4)$$

3.1.4 Surface roughness (Ra)

Concerning surface roughness, the adopted model which fits well the experimental data is the linear with interaction. The results given by the ANOVA presented in Table 9 demonstrate that r and f are the most significant terms with the respective contributions (41.83 and 35.39 %). The depth of cut (ap) appears significant with smaller contribution of 3.22 %, whereas cutting speed does not affect the surface roughness. A similar result was obtained by Aslan et al. [4] when turning AISI 4140 steel (63 HRC) with mixed ceramic tool. The interactions $ap \times r$ and $f \times r$ have a significant effects with 9.64 and 7.31 % of contributions, respectively. The determination coefficient model's R^2 is 0.9387. The Pred R^2 of 0.8335 is in reasonable agreement with the Adj R^2 of 0.9064. The final equation in terms of real factors is given as follows:

$$Ra = -0.049 + 2.242 \times 10^3 Vc - 3.618ap + 12.479f + 0.051r - 0.015Vc \times f - 6.875 \times 10^{-4} Vc \times r + 7.917ap \times f + 1.938ap \times r - 5.625f \times r \quad (5)$$

The curves of the experimental and predicted values of cutting forces and surface roughness are drawn in Figs. 2 and 3. It is seen that the predicted curves fit the experimental ones except at some run points where we can notice a small divergence.

3.2 Response surface graphic analysis

3.2.1 Cutting forces

The evolution of feed force as a function of depth of cut and cutting speed is depicted in Fig. 4. It shows that the feed force is considerably influenced by depth of cut, but when cutting speed increases, this influence is reduced. It could be explained by the material softening caused by the elevation of the cutting temperature during machining.

The effect of both depth of cut and feed rate on thrust force is presented in Fig. 5. It indicates that the thrust force increases with the increase in depth of cut. It reaches its maximum value around the middle level of depth of cut with feed rate of 0.14 mm/rev. Then, it decreases by increasing depth of cut. Additionally, we can observe that the use of feed rate in the neighborhood of 0.11 mm/rev gives the lower values of thrust force whatever the depth of cut is. It was deduced previously that both feed rate and depth of cut are statically significant.

The relationship between the tangential force and both depth of cut and feed rate is plotted in Fig. 6. As it was expected, the tangential force increases with the increase of

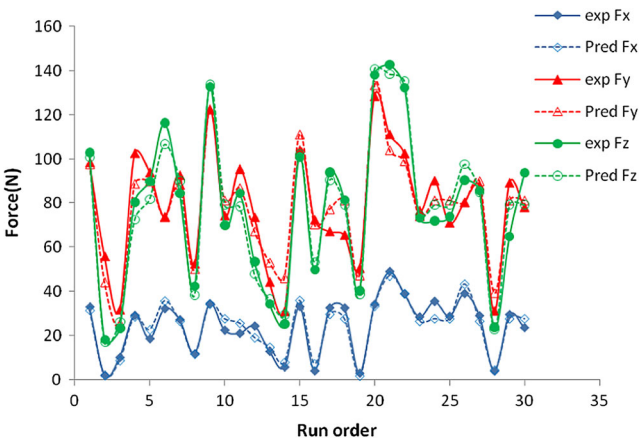

Fig. 2 Experimental and predicted cutting force values

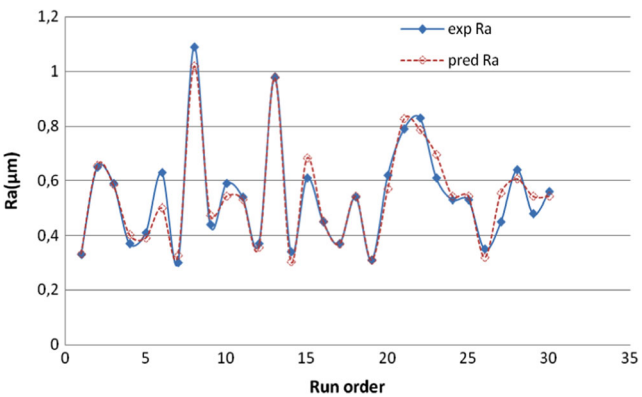

Fig. 3 Experimental and predicted surface roughness values

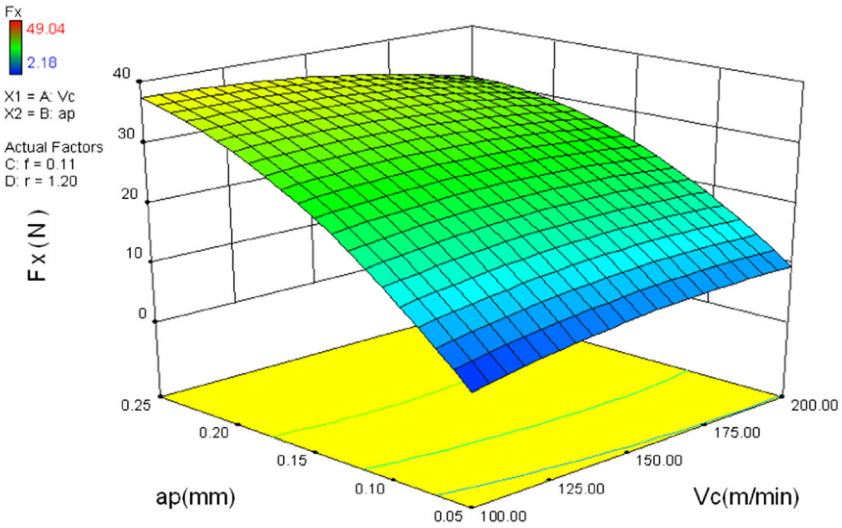

Fig. 4 Effect of depth of cut and cutting speed on feed force

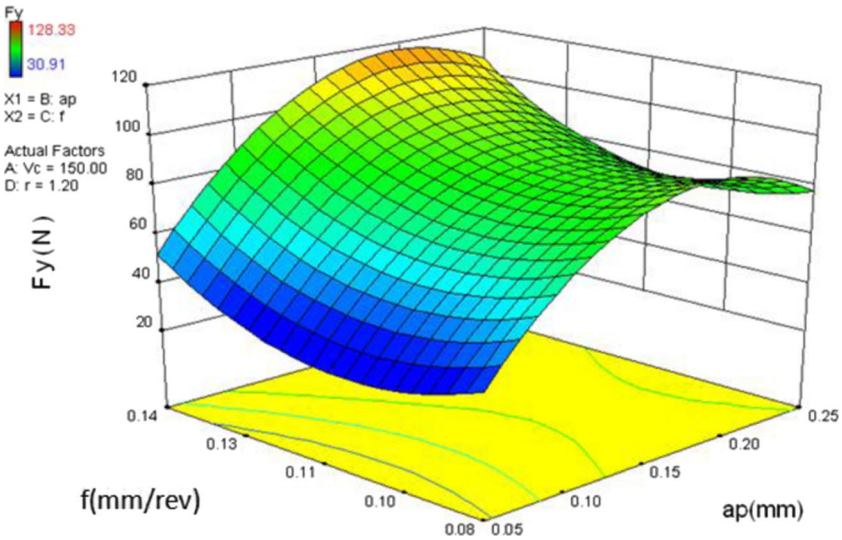

Fig. 5 Effect of depth of cut and feed rate on thrust force

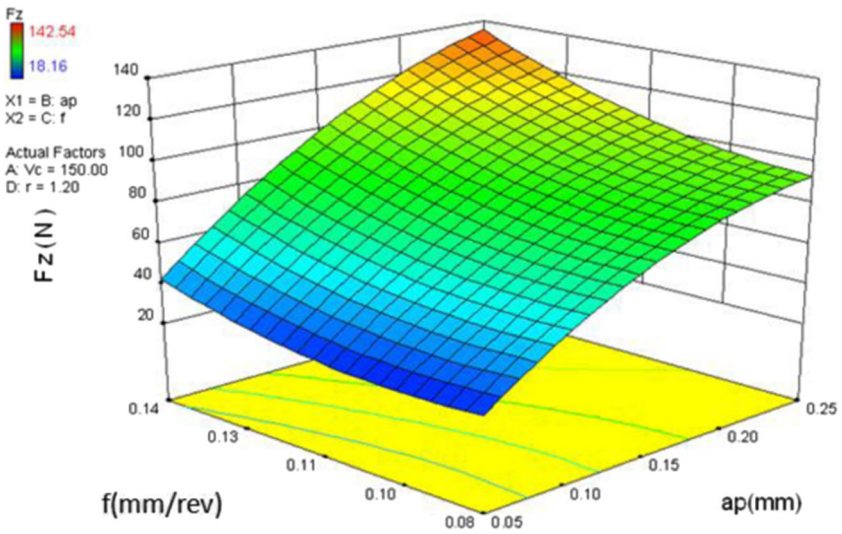

Fig. 6 Effect of depth of cut and feed rate on tangential force

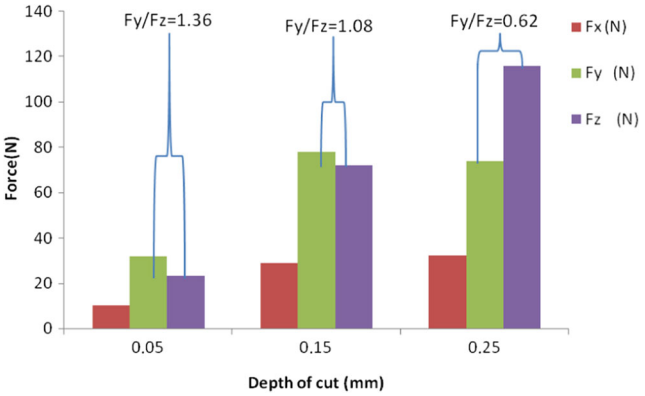

Fig. 7 Effect of depth on cutting forces in middle levels of *Vc*, *f*, and *r*

depth of cut and feed rate due to the enlargement of cutting action area.

Figure 7 represents the evolution of the cutting force components and the corresponding ratio of thrust force to tangential force (*Fy*/*Fz*) at different depths of cut. It is seen that the trust force is the predominant one at small depth of cut with a ratio of 1.36. But, when the depth of cut reaches 0.25 mm, the tangential force becomes the largest one with a ratio of 0.62.

3.2.2 Surface roughness

It is well observed according to Fig. 8 that the use of small feed rate and large nose radius results in the lowest surface roughness. As reported by Benga and Abrao [2], at small feed rate, the distance between peak and valleys of the feed marks is small. However, the use of large feed rate and small tool nose radius results in highest surface roughness.

The effect of both tool nose radius and depth of cut on surface roughness is depicted in Fig. 9. We can observe that high values of surface roughness are obtained when using

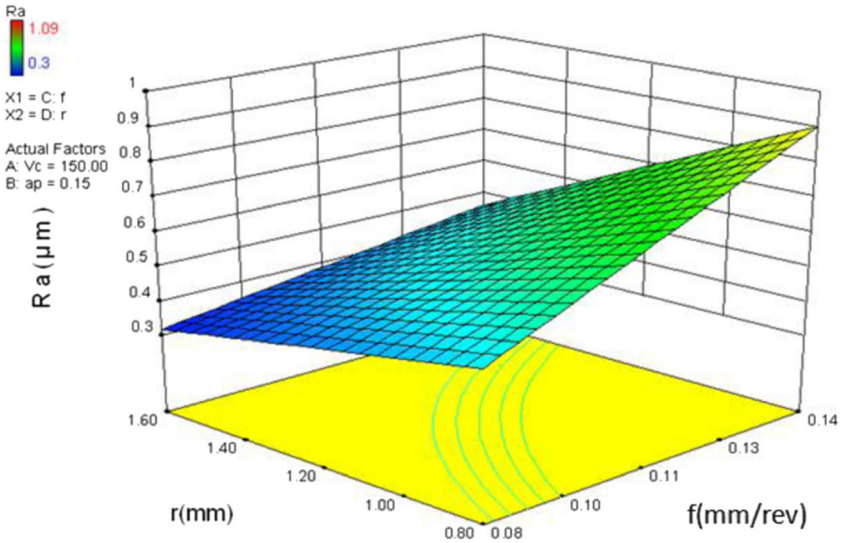

Fig. 8 Effect of tool nose radius and feed rate on surface roughness

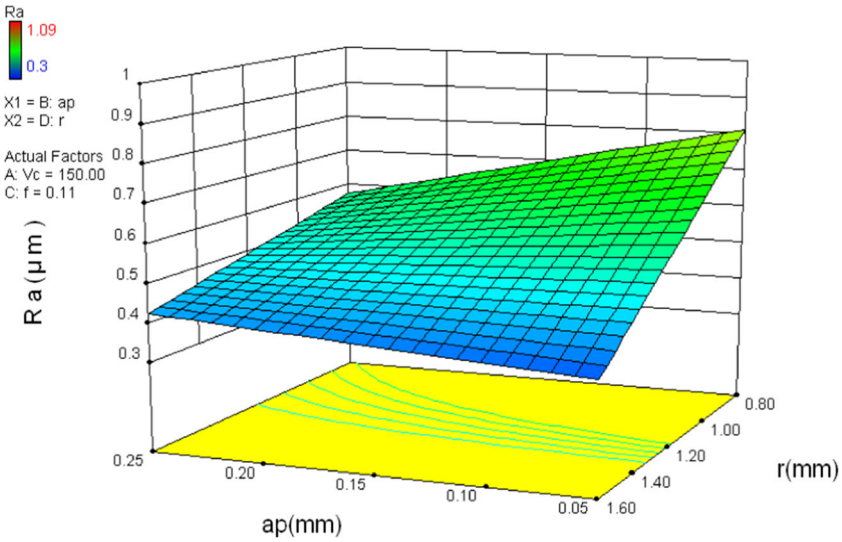

Fig. 9 Effect of tool nose radius and depth of cut on surface roughness

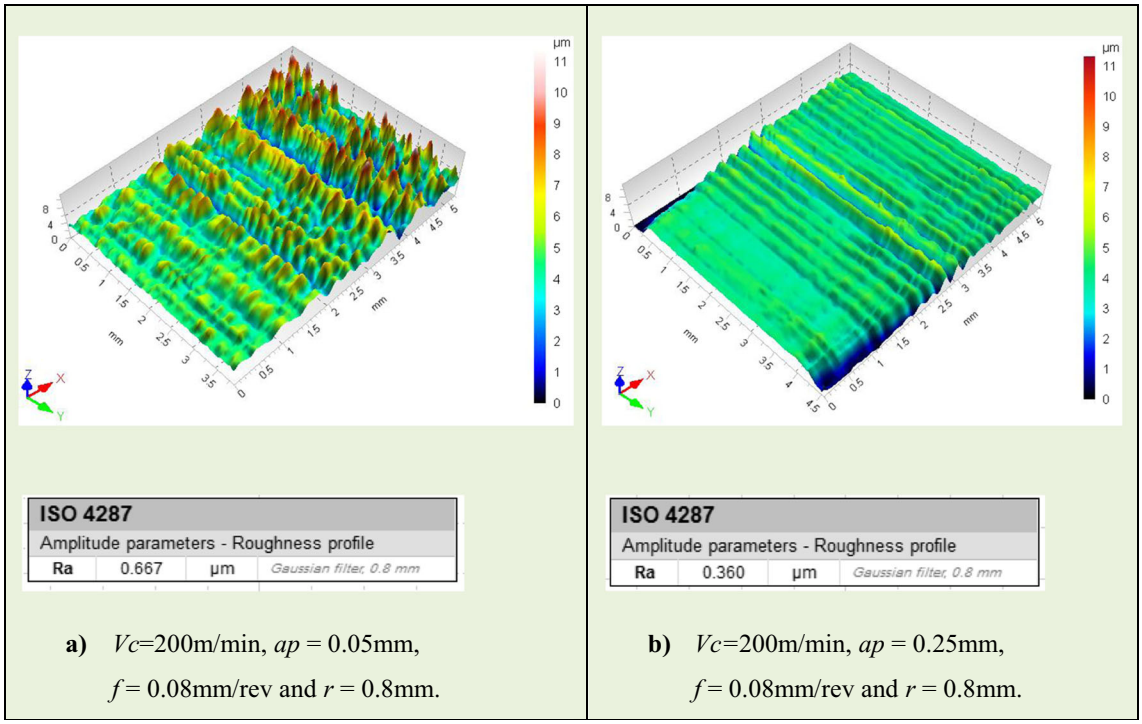

a) Vc=200m/min, ap = 0.05mm, f = 0.08mm/rev and r = 0.8mm.

b) Vc=200m/min, ap = 0.25mm, f = 0.08mm/rev and r = 0.8mm.

Fig. 10 Topographies of AISI 52100 steel hard turned with mixed ceramic insert

small depth, especially with tool nose radius of 0.8 mm. We could attribute this to the material side flow phenomenon which is characterized by the elevation of temperature and specific cutting pressure in the cutting zone when using small undeformed chip thickness. It consists of ploughing and squeezing of the machined material by the tool causing its deterioration [24]. Figure 10a, b shows the topographies of machined surfaces using the lower feed rate and with both values of depth of cut (0.05 and 0.25), respectively.

To well illustrate the comparison of the two surfaces, a portion of the surface (a) is superimposed on surface (b) as well as the feed marks of both surfaces are parallel (Fig. 11). We can observe that the valleys of surface (a) are distant above those of surface (b) due to the material accumulation. This additional volume of squeezed material presses on the tool flank face, which could contribute to the dominance of thrust force at small depth of cut mentioned in the precedent subsection. We have to note that the ratio

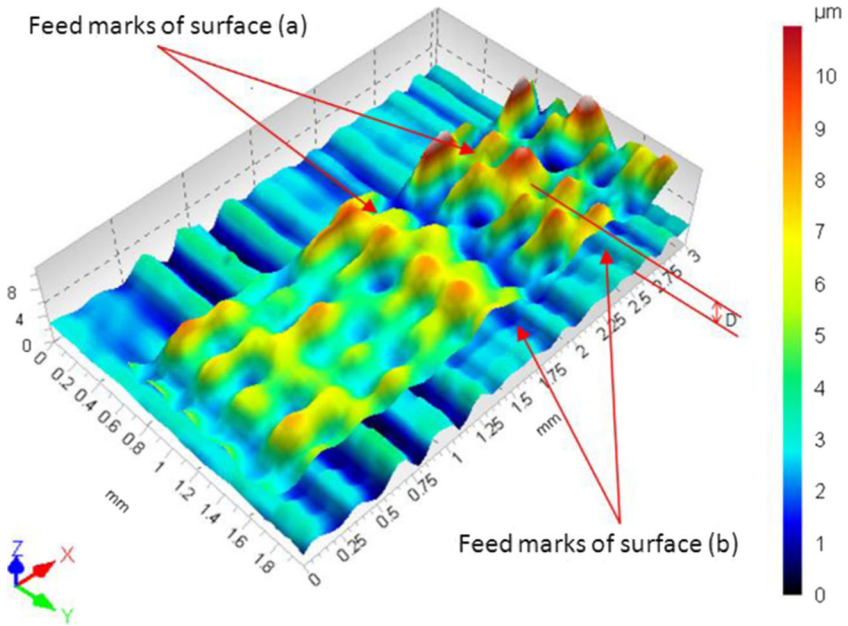

Fig. 11 Comparison between surface (*a*) and surface (*b*) topographies

Table 10 Comparison between experimental and predicted values

Run	*Vc* (m/min)	*ap* (mm)	*f* (mm/rev)	*r* (mm)	Response	Experimental	Predicted	Error (%)
1	115.4	0.05	0.09	1.60	*Fx* (N)	3.05	3.56	16.72
2	131.9	0.20	0.09	0.80		35.12	35.19	0.20
3	160.9	0.10	0.12	1.20		20.29	21.11	4.03
1	115.4	0.05	0.09	1.60	*Fy* (N)	40.13	39.80	−0.82
2	131.9	0.20	0.09	0.80		81.02	81.45	0.53
3	160.9	0.10	0.12	1.20		69.12	69.08	−0.05
1	115.4	0.05	0.09	1.60	*Fz* (N)	31.21	34.23	9.69
2	131.9	0.20	0.09	0.80		84.23	85.75	1.80
3	160.9	0.10	0.12	1.20		58.32	60.25	3.31
1	115.4	0.05	0.09	1.60	*Ra* (μm)	0.34	0.33	−2.78
2	131.9	0.20	0.09	0.80		0.48	0.48	0.68
3	160.9	0.10	0.12	1.20		0.64	0.60	−5.78

Table 11 Constraints for optimization of machining parameters

Name	Goal	Lower limit	Upper limit
Vc (m/min)	In range	100	200
ap (mm)	In range	0.05	0.25
f (mm/rev)	In range	0.08	0.14
r (mm)	In range	0.8	1.6
Fx (N)	Minimize	2.18	49.04
Fy (N)	Minimize	30.91	128.33
Fz (N)	Minimize	18.16	142.54
Ra (μm)	Minimize	0.3	1.09

(*Fy*/*Fz*) of surface (a) is four times greater than the surface (b) ratio.

3.3 Model confirmation

The reliability of the developed mathematical models is investigated by performing three new runs. The confirmation run conditions were set within the range of the factor levels already defined. The first run corresponds to the most desirable response. The two others were conducted randomly. Table 10 shows the percentage error between the experimental values and their corresponding predicted values obtained from the Eqs. 2–5. The maximum divergence 16.72 % was found for small feed force of 3.05 N which is negligible comparing to thrust and tangential force in hard turning, whereas the slight values of divergence were observed for thrust force, tangential force, and surface roughness. Consequently, the mathematical models can be used to effectively predicting the cutting force components and surface roughness values for any combination of cutting speed, feed rate, depth of cut, and tool nose radius within the limits of the actual experimentation.

4 Optimization

The choice of the desired goal for each factor and response was done as well as minimizing power consumption through cutting forces and minimizing surface roughness. Desirability function approach was used for multiple response factor (*Fx*, *Fy*, *Fz*, and *Ra*) optimization. The optimization process seeks for a combination of factor levels that simultaneously satisfy the desired goals. Table 11 presents the constraints applied during the optimization process. The optimal solutions are reported in Table 12 in decreasing order of desirability level.

Table 12 Optimization solutions

Number	*Vc* (m/min)	*ap* (mm)	*f* (mm/rev)	*r* (mm)	*Fx* (N)	*Fy* (N)	*Fz* (N)	*Ra* (μm)	Desirability
1	115.40	0.05	0.09	1.60	2.18	39.62	33.05	0.33	0.937
2	116.08	0.05	0.09	1.60	2.19	39.21	33.36	0.33	0.937
3	114.22	0.05	0.09	1.60	2.18	40.45	32.48	0.33	0.937
4	115.00	0.05	0.09	1.60	2.18	39.87	32.93	0.33	0.937
5	116.79	0.05	0.09	1.60	2.25	39.08	33.44	0.33	0.936
6	118.29	0.05	0.09	1.60	2.30	38.21	34.20	0.34	0.936

5 Conclusion

Through the results obtained above, the following conclusions could be drawn:

1. The ANOVA results prove that the depth of cut is the main parameter affecting the force components followed by feed rate with a smaller contribution. Though, the cutting speed is not found significant, and the tool nose radius influences only the thrust force. Furthermore, it is revealed that the interaction $Vc \times ap$ is significant on feed force and that the quadratic term $ap \times ap$ is particularly significant on thrust force.
2. When using small undeformed chip thickness, the exerted pressure of the squeezed material on the tool flank face could contribute to the dominance of thrust force. Conversely, the increase in depth of cut leads to the decrease of squeezed material phenomena and to the dominance of the tangential force.
3. The best surface roughness is obtained by using small feed rate and large nose radius and the opposite is true. Moreover, it is revealed that the use of depth of cut of 0.05 mm with tool nose radius of 0.8 mm gives high surface roughness values due to the material side flow phenomenon.
4. Small divergence is observed between the predicted and the confirmation test values. Therefore, the response surface models can be used for predicting cutting forces and surface roughness values by varying the cutting conditions within the range of the actual experimentation.
5. The optimization process is done by minimizing both power consumption and surface roughness. It depends on the following factor combinations: ap=0.05 mm, f= 0.09 mm/rev, r=1.6 mm, and Vc ranged from 115.40 to 118.29 m/min.
6. The optical platform of metrology modular is an important tool in surface roughness investigation by virtue of the produced three-dimensional topographic maps of the machined surfaces.

Acknowledgments This work was achieved in the laboratory LMS (Guelma University, Algeria). The authors would like to thank the Algerian Ministry of Higher Education and Scientific Research (MESRS) and the Delegated Ministry for Scientific Research (MDRS) for providing financial support through CNEPRU Research Project, Code: 0301520080027.

References

1. Smith S, Melkote SN, Lara-Curzio E, Watkins TR, Allard L, Riester L (2007) Effect of surface integrity of hard turned AISI 52100 steel on fatigue performance. Mater Sci Eng, A 459(1–2):337–346
2. Benga GC, Abrao AM (2003) Turning of hardened 100Cr6 bearing steel with ceramic and PCBN cutting tools. J Mater Process Technol 143:237–241
3. Kacal A, Yildirim F (2013) Application of grey relational analysis in high-speed machining of hardened AISI D6 steel. Proc IMechE part C: J Mec Eng Sci 227(7):1566–1576
4. Aslan E, Camuscu N, Birgoren B (2007) Design optimization of cutting parameters when turning hardened AISI 4140 steel (63 HRC) with Al_2O_3 + TiCN mixed ceramic tool. Mater Des 28:1618–1622
5. Dureja JS, Gupta VK, Sharma VS, Dogra M (2009) Design optimization of cutting conditions and analysis of their effect on tool wear and surface roughness during hard turning of AISI-H11 steel with a coated–mixed ceramic tool. J Eng Manuf 223(B):1441–1453
6. Ozel T, Karpat Y, Figueira L, Davim JP (2007) Modeling of surface finish and tool flank wear in turning of AISI D2 steel with ceramic wiper inserts. J Mater Process Technol 189:192–198
7. Bartarya G, Choudhuryb SK (2012) Effect of cutting parameters on cutting force and surface roughness during finish hard turning AISI52100 grade steel. Procedia CIRP 1:651–656
8. Paiva AP, Campos PH, Ferreira JR, Lopes LGD, Paiva EJ, Balestrassi PP (2012) A multivariate robust parameter design approach for optimization of AISI 52100 hardened steel turning with wiper mixed ceramic tool. J Refract Met Hard Mater 30:152–163
9. Satyanarayana K, Gopal AV, Babu PB (2014) Analysis for optimal decisions on turning Ti-6AI-4 V with Taguchi-grey method. Proc IMechE Part C: J Mec Eng Sci 228(1):152–157
10. Thiele JD, Melkote SN (1999) Effect of cutting edge geometry and workpiece hardness on surface generation in the finish hard turning of AISI 52100 steel. J Mater Process Technol 94:216–226
11. Neseli S, Yaldız S, Türkes E (2011) Optimization of tool geometry parameters for turning operations based on the response surface methodology. Measurement 44:580–587
12. Elbah M, Yallese MA, Aouici H, Mabrouki T, Rigal J (2013) Comparative assessment of wiper and conventional ceramic tools on surface roughness in hard turning AISI 4140 steel. Measurement 46:3041–3056
13. Guddat J, M'Saoubi R, Alma P, Meyer D (2011) Hard turning of AISI 52100 using PCBN wiper geometry inserts and the resulting surface integrity. Procedia Eng 19:118–124
14. Meng L, Jun-ichiro T, Akira T (2004) Effect of tool nose radius and tool wear on residual stress distribution in hard turning of bearing steel. J Mater Process Technol 150:234–241
15. Zhou JM, Andersson M, Stahl JE (2003) The monitoring of flank wear on the CBN tool in the hard turning process. J Adv Manufact Technol 22:697–702
16. Tönshoff HK, Arendt C, Ben Amor R (2000) Cutting of hardened steel. CIRP Annals–Manufact Technol 49(2):547–566
17. Yallese MA, Chaoui K, Zeghib N, Boulanouar L, Rigal J (2009) Hard machining of hardened bearing steel using cubic boron nitride tool. J Mater Process Technol 209:1092–1104
18. Nakayama K, Arai M, Kanda T (1988) Machining characteristic of hard materials. CIRP Ann Manuf Technol 37:89–92
19. Astakhov VP (2010) Geometry of single-point turning tools and drills. Fundamentals and practical applications. Springer, London
20. Bouacha K, Yallese MA, Mabrouki T, Rigal J (2010) Statistical analysis of surface roughness and cutting forces using response surface methodology in hard turning of AISI 52100 bearing steel with CBN tool. J Refract Met Hard Mater 28:349–361
21. Chou YK, Song H (2004) Tool nose radius effects on finish hard turning. J Mater Process Technol 148(2):259–268
22. Kurt A, Seker U (2005) The effect of chamfer angle of polycrystalline cubic boron nitride cutting tool on the cutting forces and the tool stresses in finishing hard turning of AISI 52100 steel. Mater Des 26:351–356
23. Bagawade AD, Ramdasi PG, Pawade RS, Bramhankar PK (2012) Evaluation of cutting forces in hard turning of AISI 52100 steel by using Taguchi method. J Eng Res Technol 1(6):2278–0181
24. Kishawy HA, Elbestawi MA (1999) Effects of process parameters on material side flow during hard turning. J Mach Tools Manuf 39: 1017–1030